Chinese Journal of Chemical Engineering 53 (2023) 83–88

Contents lists available at ScienceDirect

Chinese Journal of Chemical Engineering

journal homepage: www.elsevier.com/locate/CJChE

Full Length Article

An optimization method for enhancement of gas–liquid mass transfer in a bubble column reactor based on the entropy generation extremum principle

Chao Zhang [1,*], Youzhi Liu [1], Weizhou Jiao [1], Hongyan Shen [1], Xigang Yuan [2,*], Shengkun Jia [2]

[1] Shanxi Province Key Laboratory of Higee-Oriented Chemical Engineering, North University of China, Taiyuan 030051, China
[2] State Key Laboratory for Chemical Engineering, School of Chemical Engineering and Technology, Tianjin University, Tianjin 300072, China

ARTICLE INFO

Article history:
Received 29 November 2021
Received in revised form 13 January 2022
Accepted 21 January 2022
Available online 31 January 2022

Keywords:
Entropy generation
Bubble column reactor
Optimization
Biodegradation
Flow field

ABSTRACT

In this study, an optimization method is proposed to enhance the gas–liquid mass transfer in bubble column reactor based on the entropy generation extremum principle. The mass transfer–induced entropy generation can be maximized with the increase of mass transfer rate, based on which the velocity field can be optimized. The oxygen gas–liquid mass transfer is the major rate–limiting step of the toluene emissions biodegradation process in bubble column reactor, so the entropy generation due to oxygen mass transfer is used as the objective function, and the conservation equations of the gas–liquid flow and species concentration are taken as constraints. This optimization problem is solved by the calculus of variations, the optimal liquid flow pattern is obtained and the relationship of the maximum mass transfer enhancement on viscous dissipation is revealed, which can be used to improve the design of internal structure of the bubble column reactor.

1. Introduction

The industrial waste gases containing volatile organic compounds (VOCs) such as toluene, methanal and styrene can cause severe air pollution and thus represent a potential human health hazard [1–3]. Biodegradation is expected to be more suitable than traditional physical and chemical methods for the treatment of industrial waste gas in low concentrations due to its advantages of low cost, high efficiency and no secondary environmental pollution [4,5], and the bubble column reactor is often used for biodegradation of waste gas as it can provide high gas–liquid contact and high heat and mass transfer rates at low cost [6–8]. For instance, Hecht *et al.* [9] used a bubble column reactor for biodegradation of trichloroethylene in the waste gas. Tokumura *et al.* [7] studied the dynamic performance of photo-Fenton degradation process of toluene emissions in a bubble column reactor. Wang *et al.* [10] used *Pseudomonas putida* to treat toluene emissions in a bubble column and established a computational fluid dynamics (CFD) model to predict the liquid velocity and concentration distributions, and the results revealed that the oxygen gas–liquid mass transfer was the rate-limiting step of the biodegradation process.

Many attempts have been made to enhance the efficiency of the bubble column reactor by increasing the gas–liquid mass transfer rate [11,12]. Al-Mashhadani *et al.* [13] dispersed the gas into microbubbles in a bioreactor by fluidic oscillation, which dramatically increased the available interfacial area for mass transfer and the liquid circulation for mixing. Bannari *et al.* [14] installed an impeller in the middle of the bioreactor to enhance the gas–liquid mass transfer. Wadaugsorn *et al.* [15] installed a draft tube in the bubble column to improve the mixing and mass transfer, and the size and position of the draft tube were optimized by CFD simulations. However, it should be noted that the gas–liquid mass transfer rate is increased in most studies by improving the liquid phase flow pattern, which relies on the analysis of the performance feedback data from either experiments or numerical simulations. Obviously, such an approach can effectively improve the gas–liquid mass transfer in the bubble column but can hardly find the flow pattern that gives the highest interfacial mass transfer rate.

The entropy generation extremum principle has been successfully applied to enhance fluid flow and heat and mass transfer [16–19]. Li *et al.* [20] developed an optimization method based on the entropy generation extremum principle to enhance the heat transfer in a solar receiver. Cao *et al.* [21] found that maximization

* Corresponding authors.
E-mail addresses: zhangchao1213@nue.edu.cn (C. Zhang), yuanxg@tju.edu.cn (X. Yuan).

https://doi.org/10.1016/j.cjche.2022.01.018
1004-9541/

of entropy generation due to reaction and heat transfer could enhance the solar thermal decomposition of methane, and there existed an optimal flow field that could be found at fixed viscous dissipation. In addition, Jia *et al.* [22] showed that the entropy generation extremum principle was capable of giving the thermodynamic limit for the mass transfer enhancement, and the mass transfer-induced entropy generation should be minimized for a fixed mass flux boundary condition but maximized for an isoconcentration boundary condition, respectively. In this study, a flow pattern optimization method based on the entropy generation extremum principle is firstly established to enhance the gas–liquid mass transfer in bubble column reactor, and the optimal liquid flow field is obtained at a given mechanical energy input.

In the following sections, a CFD model is established to simulate the biodegradation process of toluene emissions in a bubble column reactor, and then an optimization problem is formulated for this process. The entropy generation due to the mass transfer of dissolved oxygen is taken as the objective function, and the conservation equations of the gas–liquid flow and species concentrations are taken as constraints. This problem is solved by calculus of variations. The optimized flow patter and species concentration distributions are compared with that obtained without optimization. At last, the relationship between viscous dissipation and removal efficiency is discussed and some conclusions are drawn.

2. Model Formulation and Optimization Method

The bubble column reactor used in this study is schematically shown in Fig. 1, where the height is 1400 mm and the width is 120 mm. In the experiment, the liquid depth is 1200 mm from the reactor bottom, and the waste gas is injected into the reactor from the bottom through an inlet with a width of 50 mm. After that, toluene is absorbed in the liquid phase and then degraded into carbon dioxide and water by the suspended microorganism *Pseudomonas putida* WQ-03. The experimental data have been reported by Wang *et al.* [10].

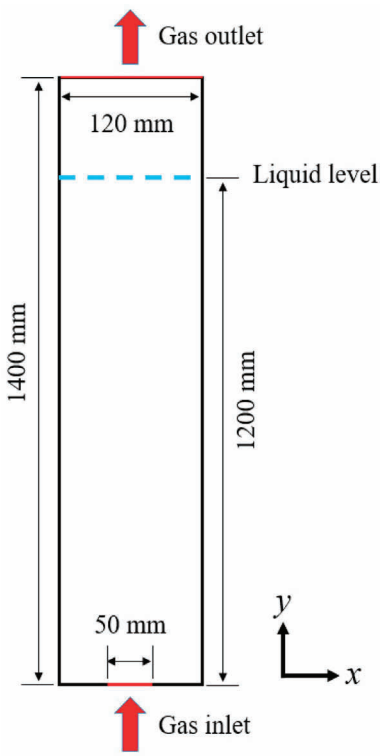

Fig. 1. A schematic diagram of the bubble column reactor.

2.1. Governing equations

2.1.1. Continuity equation

Because of the small quantity of toluene in the effluent gas, the gas–liquid mass transfer is expected to have a negligible effect on mass balance. The steady state continuity equation for gas and liquid phases is given below:

$$\frac{\partial(\alpha_k\rho_k U_{k,i})}{\partial x_i}=0 \tag{1}$$

where the subscript k denotes the phase (G refers to the gas phase and L refers to the liquid phase), the subscript i denotes the direction (j refers to another direction), U is the velocity, α is the volume fraction, and ρ is the density.

2.1.2. Momentum conservation equation

$$\frac{\partial(\alpha_k\rho_k U_{k,i}U_{k,j})}{\partial x_j}=\frac{\partial}{\partial x_i}\left[\frac{\mu_k}{\rho_k}\frac{\partial(\alpha_k\rho_k U_{k,i})}{\partial x_i}-\alpha_k\rho_k\overline{u_{k,i}u_{k,j}}\right]-\alpha_k\frac{\partial P}{\partial x_i}+\alpha_k\rho_k g+\boldsymbol{M}_k \tag{2}$$

where P, μ, $\boldsymbol{u}$ is the pressure, viscosity, fluctuating velocity respectively, and $\boldsymbol{M}_k$ accounts for the gas–liquid interfacial force. The turbulence effect is calculated by the RNG k–ε model [23]. The drag force and lift force are considered to calculate the interphase forces $\boldsymbol{M}_k$ in this work:

$$\boldsymbol{M}_L^d=-\boldsymbol{M}_G^d=\frac{3}{4}\frac{C_d}{d_{32}}\alpha_G\rho_L\left|U_{G,i}-U_{L,i}\right|\left(U_{G,i}-U_{L,i}\right) \tag{3}$$

$$\boldsymbol{M}_L^l=-\boldsymbol{M}_G^l=\alpha_G\rho_L C_l\left(U_{G,i}-U_{L,i}\right)(\nabla\times\boldsymbol{U}_L) \tag{4}$$

The superscript d and l represent the drag force and the lift force respectively, C_d is the drag coefficient and C_l is the lift coefficient. The value of C_l is taken as 0.5 [10] and the model proposed by Ishii and Zuber [24] is used to calculate the C_d. d_{32} is the gas phase Sauter bubble diameter, which is calculated by the population balance (PB) model [25].

2.1.3. Species conservation equation

The species i of toluene/oxygen in the gas/liquid phase is represented by its mass fraction C^i.

$$\frac{\partial(\alpha_G\rho_G U_{G,i}C_G^t)}{\partial x_i}=\frac{\partial}{\partial x_i}\left(\alpha_G\rho_G D_{G,\mathrm{eff}}^t\frac{\partial C_G^t}{\partial x_i}\right)-K_{LG}^t a\rho_L\left(C_L^{t*}-C_L^t\right) \tag{5}$$

$$\frac{\partial(\alpha_L\rho_L U_{L,i}C_L^t)}{\partial x_i}=\frac{\partial}{\partial x_i}\left(\alpha_L\rho_L D_{L,\mathrm{eff}}^t\frac{\partial C_L^t}{\partial x_i}\right)+S^t+K_{LG}^t a\rho_L\left(C_L^{t*}-C_L^t\right) \tag{6}$$

$$\frac{\partial(\alpha_L\rho_L U_{L,i}C_L^o)}{\partial x_i}=\frac{\partial}{\partial x_i}\left(\alpha_L\rho_L D_{L,\mathrm{eff}}^o\frac{\partial C_L^o}{\partial x_i}\right)+S^o+K_{LG}^o a\rho_L\left(C_L^{o*}-C_L^o\right) \tag{7}$$

$$\frac{\partial(\alpha_L\rho_L U_{L,i}C_L^x)}{\partial x_i}=S^x \tag{8}$$

where the superscripts t, o and x denote the toluene, oxygen and biomass, respectively. C^{i*} is the equilibrium mass fraction of species i in the liquid phase, a is the interfacial area, and D_{eff}^i is the effective mass diffusivity of species i. Given the low gas–liquid mass transfer rate of oxygen and the low variation (within 10%) of gas phase pressure in the bubble column, the gas phase oxygen concentration is assumed to be a constant. $S=\alpha_L r$ is the source term for the bioreaction, and r is the reaction rate. The eddy cell model [26] is adopted

to calculate the gas–liquid mass transfer coefficient K_{LG}^{i} in this work.

2.1.4. Microbial kinetics

The biomass is assumed to possess a substrate–inhibited response to the dissolved toluene and a Monod–type response to the dissolved oxygen [27]. The bioreaction rate of the biomass r^{x} is expressed as follows [28,29]:

$$r^{x}=\frac{\mathrm{d}(\rho_{L}C_{L}^{x})}{\mathrm{d}t}=\frac{\mu_{max}p_{L}C_{L}^{t}}{K^{t}+p_{L}C_{L}^{t}+(p_{L}C_{L}^{t})^{2}/K_{I}}\cdot\frac{p_{L}C_{L}^{o}}{K^{o}+p_{L}C_{L}^{o}}\cdot\rho_{L}C_{L}^{x} \tag{9}$$

where μ_{max} is the maximum specific growth rate, K^{t} and K^{o} are the half–saturation constants for toluene and oxygen, and K_{I} is the inhibitory constant for toluene. In addition, the degradation rate of toluene, r^{t}, is calculated by

$$r^{t}=\frac{\mathrm{d}(\rho_{L}C_{L}^{t})}{\mathrm{d}}=-\frac{1}{Y_{xt}}r^{x} \tag{10}$$

where the constant Y_{xt} is the yield coefficient.

The value of K^{o} is obtained from the study of Ref. [28], while the values of μ_{max}, K^{t}, K_{I}, and Y_{xt} are obtained from the batch experiment [10], as shown in Table 1.

The biodegradation products of toluene are assumed to consist of cells, CO_2, and H_2O, and the bioreaction can be written as [30]:

$$C_7H_8+6.88O_2+0.41NH_3\rightarrow 2.05CH_{1.84}O_{0.55}N_{0.2}(\text{biomass})+4.95CO_2+2.73H_2O \tag{11}$$

According to the above equation, the consumption rate of dissolved oxygen is 2.39 times that of dissolved toluene. And the oxygen reaction rate r^{o} can be calculated as follows:

$$r^{o}=2.39r^{t} \tag{12}$$

2.2. Optimization method

As the gas–liquid mass transfer of oxygen is the rate-limiting step of the biodegradation process [10], a liquid flow field optimization method is proposed in this section based on the entropy generation extremum principle to enhance the gas–liquid mass transfer rate of oxygen to its thermodynamic limit under the condition of fixed viscous dissipation. The momentum conservation equation for the liquid phase is given below:

$$\frac{\partial(\alpha_{L}\rho_{L}U_{L,i}U_{L,j})}{\partial x_{j}}=\frac{\partial}{\partial x_{i}}\left[\frac{\mu_{L,eff}}{\rho_{L}}\frac{\partial(\alpha_{L}\rho_{L}U_{L,i})}{\partial x_{i}}\right]-\alpha_{L}\frac{\partial P}{\partial x_{i}}+\alpha_{L}\rho_{L}g+\boldsymbol{M}_{L}+\boldsymbol{F} \tag{13}$$

where $\boldsymbol{F}$ is the external force reserved for the optimization method, and in order to determine the optimum value of $\boldsymbol{F}$, the optimization problem with the entropy generation of oxygen mass transfer in the liquid phase as the objective function is solved for the liquid velocity field and the associated external force field. The optimization is performed with the constraints of fixed liquid–phase viscous dissipation.

According to our previous work [22], in order to enhance the mass transfer under the isoconcentration condition, the total entropy generation should be maximized when solving the optimization problem. As the oxygen concentration at the gas–liquid interface remains unchanged in the biodegradation of toluene in the bubble column reactor, the boundary condition for the mass transfer of dissolved oxygen in the liquid phase is taken to be the isoconcentration condition, and in order to enhance the mass transfer of dissolved oxygen in the liquid phase, the total entropy generation due to mass transfer should be maximized. The entropy generation by the mass transfer of dissolved oxygen S_{ge} is expressed as follows [22]:

$$S_{ge}=\frac{\rho_{L}^{2}RD_{L,eff}}{M_{O_2}M_{H_2O}C_{M}C_{L}^{o}(1-C_{L}^{o})}\left(\frac{\partial C_{L}^{o}}{\partial x_{i}}\right)^{2} \tag{14}$$

where C_M is the total molar concentration in the liquid phase, and the integral of S_{ge} is taken as the objective function:

$$\max J=\iiint_{\Omega}S_{ge}\mathrm{d}V \tag{15}$$

where J is a function of the dissolved oxygen concentration C_{L}^{o} and its gradient. The continuity (Eq. (1)), momentum conservation (Eq. (13)), and species conservation (Eqs. (5)–(8)) should be satisfied in the mass transfer process. In addition, the total liquid phase viscous dissipation in the bubble column reactor is constrained to a constant, which is given by Eq. (16):

$$\iiint_{\Omega}\phi_{L}\mathrm{d}V=\text{const} \tag{16}$$

where ϕ_L is the local liquid phase viscous dissipation:

$$\phi_{L}=\mu_{L,eff}\frac{\partial U_{i}}{\partial x_{j}}\left(\frac{\partial U_{i}}{\partial x_{j}}+\frac{\partial U_{j}}{\partial x_{i}}\right) \tag{17}$$

Thus, the problem is to maximize the objective function J described in Eq. (15). Then, the constraints are incorporated into the objective function by Lagrange multiplies:

$$\prod=\iiint_{\Omega}\left\{\frac{\rho_{L}^{2}RD_{L,eff}}{M_{O_2}M_{H_2O}C_{M}C_{L}^{o}(1-C_{L}^{o})}\left(\frac{\partial C_{L}^{o}}{\partial x_{i}}\right)^{2}+C_{s}\phi_{L}+B\left[\frac{\partial(\alpha_{L}\rho_{L}U_{L,i})}{\partial x_{i}}\right]+A\left[\frac{\partial}{\partial x_{i}}\left(\rho_{L}\alpha_{L}D_{L,eff}^{o}\frac{\partial C_{L}^{o}}{\partial x_{i}}\right)-\frac{\partial(\rho_{L}\alpha_{L}U_{L,i}C_{L}^{o})}{\partial x_{i}}+S^{o}+K_{LG}^{o}a\rho_{L}(C_{L}^{o*}-C_{L}^{o})\right]\right\}dV \tag{18}$$

where A, B and C_s are Lagrange multipliers, in which C_s is a constant, while A and B are variables that vary with position. The optimization problem can be solved by calculus of variations.

The variation of Eq. (18) with respect to C_{L}^{o} is given by:

$$-\frac{\partial(\rho_{L}\alpha_{L}U_{L,i}A)}{\partial x_{i}}=\frac{\partial}{\partial x_{i}}\left(\rho_{L}\alpha_{L}D_{L,eff}^{o}\frac{\partial A}{\partial x_{i}}\right)+A\left(\frac{\partial S^{o}}{\partial C_{L}^{o}}-K_{LG}^{o}a\rho_{L}\right)+\frac{\rho_{L}^{2}RD_{L,eff}}{M_{O_2}M_{H_2O}C_{M}}\left[\frac{D_{L,eff}(1-2C_{L}^{o})}{C_{L}^{o2}(1-C_{L}^{o})^{2}}\left(\frac{\partial C_{L}^{o}}{\partial x_{i}}\right)^{2}-2\frac{D_{L,eff}}{C_{L}^{o}(1-C_{L}^{o})}\frac{\partial}{\partial x_{i}}\left(\frac{\partial C_{L}^{o}}{\partial x_{i}}\right)\right] \tag{19}$$

The variation of Eq. (18) with respect to U is given by:

$$\frac{\partial}{\partial x_{i}}\left[\frac{\mu_{L,eff}}{\rho_{L}}\frac{\partial(\alpha_{L}\rho_{L}U_{L,i})}{\partial x_{i}}\right]+\frac{\alpha_{L}}{2C_{s}}\frac{\partial B}{\partial x_{i}}+\frac{1}{2C_{s}}A\alpha_{L}\rho_{L}\frac{\partial C_{L}^{o}}{\partial x_{i}}=0 \tag{20}$$

Comparison of Eq. (20) with Eq. (13) yields:

$$\frac{\alpha_{L}}{2C_{s}}\frac{\partial B}{\partial x_{i}}=-\alpha_{L}\frac{\partial P}{\partial x_{i}}+\alpha_{L}\rho_{L}g+\boldsymbol{M}_{L} \tag{21}$$

$$\boldsymbol{F}=\frac{\partial(\alpha_{L}\rho_{L}U_{L,i}U_{L,j})}{\partial x_{j}}+\frac{1}{2C_{s}}A\alpha_{L}\rho_{L}\frac{\partial C_{L}^{o}}{\partial x_{i}} \tag{22}$$

Thus, the external force $\boldsymbol{F}$ in Eq. (13) can be calculated by Eq. (22), and then the optimization problem described by Eq. (15) with constraints can be solved by solving the set of the continuity equa-

Table 1
The values of microbial kinetic constants

K^{t}/g·m^{-3}	K_{I}/g·m^{-3}	K^{o}/g·m^{-3}	Y_{xt}	μ_{max}/h^{-1}
9.6	31.4	0.26	0.57	0.28

tion (Eq. (1)), momentum conservation equation (Eq. (13)), and species conservation equations (Eqs. (5)–(8)) to obtain the optimal fields of velocity, species concentration and pressure.

3. Boundary Conditions and Numerical Solution

A velocity inlet boundary condition was applied to the inlet of the bubble column reactor, and a degassing condition was applied to the outlet [31–33]. For both gas and liquid phases, a no-slip condition was applied on the wall. The equations were solved by the finite volume method using ANSYS Fluent 14.5 in a 2D space. The continuity, momentum conservation and species conservation equations were solved using the SIMPLE algorithm and the second-order discretization scheme. The external force $\boldsymbol{F}$ was incorporated into the momentum equation by the user defined function (UDF). A grid with 84200 structured quadrilateral meshes was selected in this work after grid independence studies.

4. Results and Discussion

4.1. Model validation

Fig. 2 shows the simulated and experimental removal efficiency of toluene (RE) at different toluene loadings. It is seen that RE is decreased with the increase of the loading from 1 to 4 g·m^{-3}, and there is a good agreement between the simulated results obtained by the proposed model and the experimental results of Wang *et al.* [10], which verifies that the model described in Section 2.1 could well describe the biodegradation process of toluene in a bubble column reactor. The optimization is performed at a superficial gas velocity of 0.01 m·s^{-1} and a toluene loading of 15 g·m^{-3} by the method proposed in Section 2.2.

4.2. Comparison between optimized and non-optimized results

CFD simulations of the biodegradation process of toluene in a bubble column reactor with or without optimization were carried out, and their streamlines and dissolved oxygen distributions were compared, as shown in Figs. 3 and 4. A comparison between Fig. 3 (a) and (b) reveals changes in the flow pattern of the liquid phase and formation of a large vortex in the middle of the bubble column reactor due to the external force *F*. As shown in Fig. 4, this vortex leads to the perturbation of the dissolved oxygen distribution. The maximum dissolved oxygen concentration in the liquid phase is increased from 3.19 g·m^{-3} in the case of no optimization to 3.64 g·m^{-3} in the case of optimization, and the average concentration is increased from 1.31 to 1.49 g·m^{-3}, indicating that the gas–liquid mass transfer of oxygen is significantly enhanced.

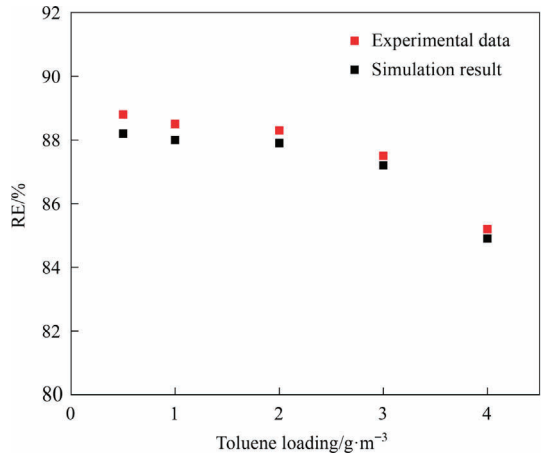

Fig. 2. Comparison between experimental and simulated removal efficiency of toluene at a superficial gas velocity of 0.01 m·s^{-1}.

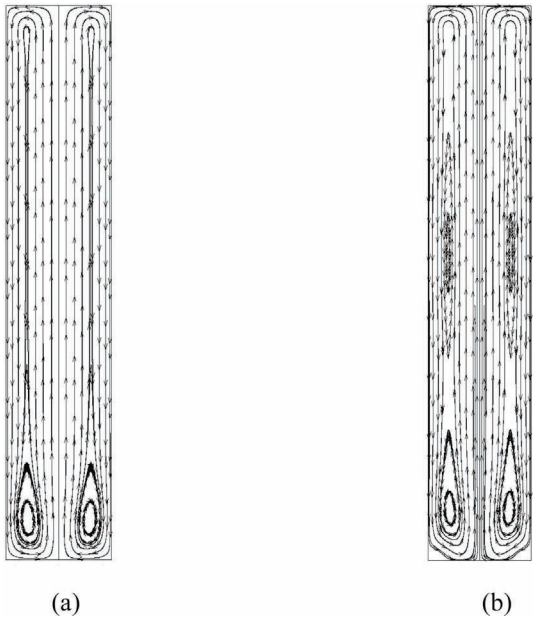

Fig. 3. The streamlines of the liquid phase in bubble column in the case of no optimization (a) and optimization (b).

The distribution of entropy generation due to mass transfer of oxygen in the liquid phase is shown in Fig. 5. Fig. 5(a) shows that entropy generation in the case of no optimization is relatively higher in the middle and lower parts of the bubble column where there exists distinct dissolved oxygen concentration gradient. Optimization leads to a significant increase in entropy generation from 0.00294 to 0.00358 W·m^{-3}·K^{-1} on average (Fig. 5(b)). Thus, the dissolved oxygen concentration gradient near the gas–liquid interface is increased, thus leading to transfer of more oxygen from the gas phase to the liquid phase and consequently an increase in the dissolved oxygen concentration in the liquid phase (Fig. 4).

According to the bioreaction model described in Section 2.1, the biodegradation rate of toluene S^t would increase as the dissolved oxygen concentration in the liquid phase increases. Fig. 6 shows

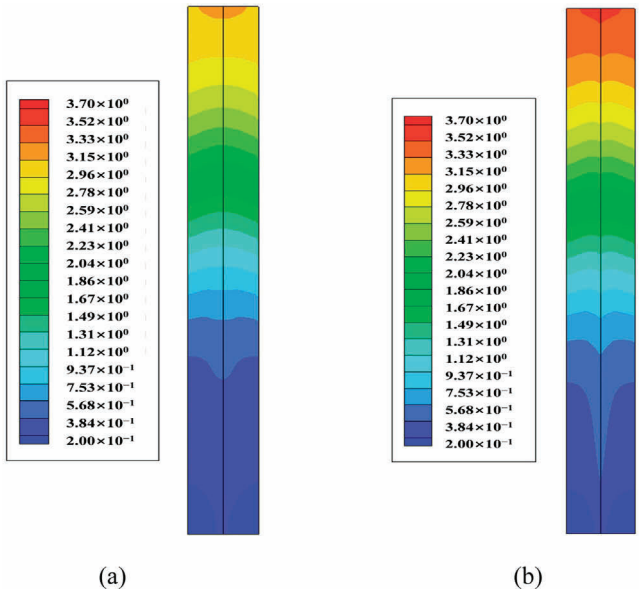

Fig. 4. The contours of the liquid phase oxygen concentration (g·m^{-3}) in the bubble column in the case of no optimization (a) and optimization (b).

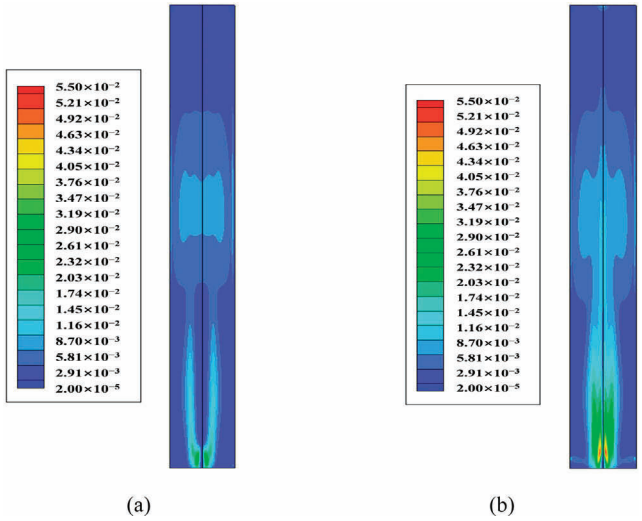

Fig. 5. The contours of entropy generation due to mass transfer of oxygen ($g \cdot m^{-3}$) in the liquid phase in the case of no optimization (a) and optimization (b).

that the average liquid phase toluene concentration is decreased from 3.45 to 3.23 $g \cdot m^{-3}$ after optimization, which could enhance the gas–liquid mass transfer driving force. As a consequence, the removal efficiency of toluene in the gas phase is increased from 79.6% to 85.5% due to the optimization of the flow field.

4.3. Relationship between viscous dissipation and oxygen mass transfer enhancement

Maximization of entropy generation is performed at a constant viscous dissipation by Eq. (12), and the Lagrange multiplier C_s is fixed to be a constant in formulating and solving the condition equation set. Then, the optimization is performed at different values of C_s, and the maximum entropy generation and associated velocity and concentration distributions can be obtained at different viscous dissipation. Fig. 7 shows the variation of the liquid phase volume-averaged entropy generation S_{ge} and dissolved oxygen concentration C^o with the increase of volume-averaged viscous dissipation ϕ_L from 9 to 12 $W \cdot m^{-3}$. It is seen that with the increase of mass transfer enhancement (*i.e.*, C^o), both volume-averaged viscous dissipation and entropy generation S_{ge} are increased, which

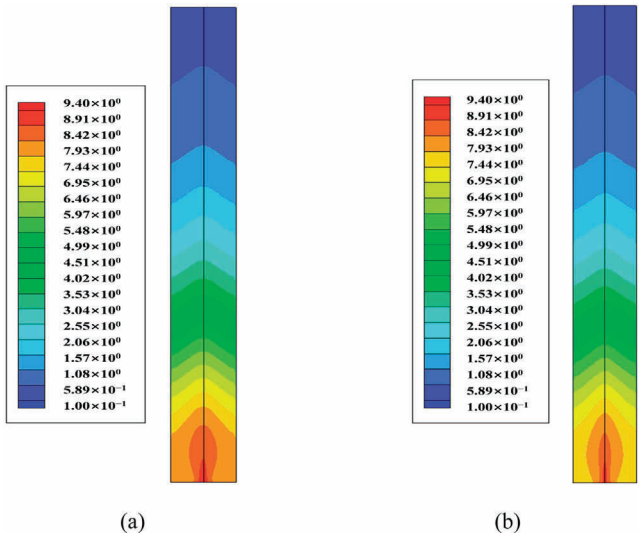

Fig. 6. The contours of the liquid phase toluene concentration ($g \cdot m^{-3}$) in the bubble column in the case of no optimization (a) and optimization (b).

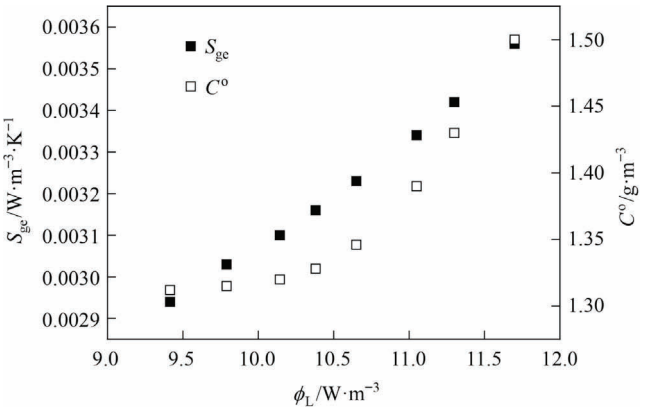

Fig. 7. Variation of the liquid phase volume-averaged entropy generation and dissolved oxygen concentration with the volume-averaged viscous dissipation.

supports the hypothesis described in Section 2.2 that the oxygen concentration at the gas–liquid interface remains unchanged in the biodegradation of toluene in a bubble column reactor and the boundary condition for oxygen mass transfer in the liquid phase can be set to be an isoconcentration condition. Thus, the volume–averaged entropy generation S_{ge} should be maximized in order to enhance the mass transfer of dissolved oxygen in the liquid phase.

4.4. Relationship between viscous dissipation and removal efficiency

Fig. 8 shows the variation of the liquid phase volume-averaged biodegradation rate of toluene S^t and its removal efficiency in the gas phase RE with the volume-averaged viscous dissipation ϕ_L. It is seen that the oxygen mass transfer and the dissolved oxygen concentration C^o increase with increasing volume-averaged viscous dissipation ϕ_L, thus leading to an increase in the biodegradation rate of toluene S^t and subsequently an increase in the removal efficiency of toluene in the gas phase RE from 79.6% in the case of no optimization to 85.5% in the case of optimization. The viscous dissipation increases with increasing mechanical energy input, and it is well-known that the mass transfer process can be enhanced by increasing the mechanical energy input. However, it should be noted that the curve shown in Fig. 8 gives a thermodynamic limit for the biodegradation process enhancement in a bubble column reactor, because the result is obtained based on the entropy generation extremum principle.

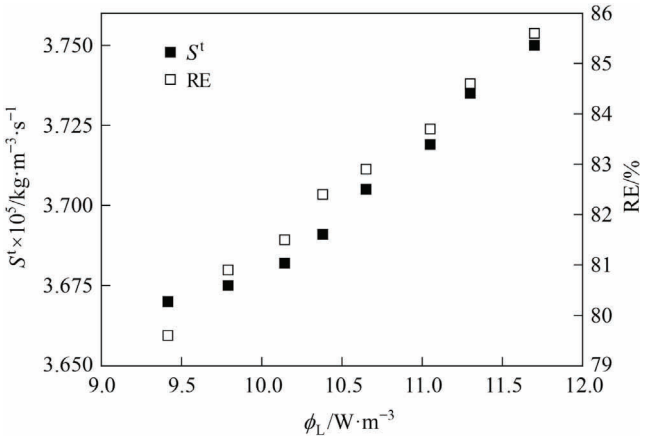

Fig. 8. Variation of the liquid phase volume-averaged biodegradation rate of toluene and its removal efficiency in the gas phase with the volume-averaged viscous dissipation.

5. Conclusions

In this study, an optimization method is proposed to enhance the biodegradation of toluene emissions in a bubble column reactor based on the reconstruction of the flow field. As the oxygen gas–liquid mass transfer is the rate-limiting step of the biodegradation process, and the oxygen concentration at the gas–liquid interface remains unchanged, maximization of entropy generation due to oxygen mass transfer in the liquid phase can enhance the oxygen mass transfer at the gas–liquid interface and consequently the biodegradation rate of toluene. There exists an optimal liquid phase flow field that can be found at a fixed viscous dissipation. An optimization problem is formulated with entropy generation due to oxygen mass transfer in the liquid phase as the objective function and all conservation equations as constraints, and it is solved by using calculus of variations. In addition, a set of condition equations are constructed to obtain the optimal solution. A thermodynamic limit is obtained by the proposed method for enhancement of oxygen mass transfer in the biodegradation process at a given viscous dissipation. As the liquid viscous dissipation is varied, the relationships of dissolved oxygen concentration and removal efficiency with viscous dissipation can be obtained. As expected, increasing the mechanical energy input can enhance the mass transfer. The optimal liquid flow pattern can be obtained by the proposed optimization method, which can provide an insight into how the flow pattern can be used to enhance the mass transfer and a guideline for designing the internal structure of the bubble column, such as the shape, position and size of the draft tube.

Declaration of Competing Interest

The authors declare that they have no known competing financial interests or personal relationships that could have appeared to influence the work reported in this paper.

Acknowledgements

This work is supported by the National Natural Science Foundation of China (91834303 and 22108261), the Open Foundation of State Key Laboratory of Chemical Engineering (SKL-ChE-19B02), Fundamental Research Program of Shanxi Province (20210302124618), and Scientific Technological Innovation Programs of Higher Education Institution in Shanxi (2020L0284).

References

[1] W. Xiang, X.Y. Zhang, K.Q. Chen, J.E. Fang, F. He, X. Hu, D.C.W. Tsang, Y.S. Ok, B. Gao, Enhanced adsorption performance and governing mechanisms of ball-milled biochar for the removal of volatile organic compounds (VOCs), *Chem. Eng. J.* 385 (2020) 123842.
[2] M. Davarpanah, M. Feizbakhshan, Z. Hashisho, D. Crompton, Process intensification in binary adsorption of VOC–water vapor on zeolite in a countercurrent fluidized bed adsorber, *Chem. Eng. J.* 423 (2021) 130225.
[3] B.H.M. Beigi, R.B. Thorpe, S. Ouki, P. Winter, A. Waalkens, Hydrogen sulphide and VOC removal in biotrickling filters: Comparison of data from a full-scale, low-emission unit with kinetic models, *Chem. Eng. Sci.* 208 (2019) 115033.
[4] E. Wantz, A. Kane, M. Lhuissier, A. Amrane, J.L. Audic, A. Couvert, A mathematical model for VOCs removal in a treatment process coupling absorption and biodegradation, *Chem. Eng. J.* 423 (2021) 130106.
[5] J.P. Wen, Y. Chen, X.Q. Jia, G.Z. Mao, Removal of toluene from air streams using a gas–liquid–solid three-phase airlift loop bioreactor containing immobilized cells, *J. Chem. Technol. Biotechnol.* 81 (1) (2006) 17–22.
[6] X.Q. Jia, X. Wang, J.P. Wen, W. Feng, Y. Jiang, CFD modelling of phenol biodegradation by immobilized Candida tropicalis in a gas–liquid–solid three-phase bubble column, *Chem. Eng. J.* 157 (2–3) (2010) 451–465.
[7] M. Tokumura, M. Shibusawa, Y. Kawase, Dynamic simulation of degradation of toluene in waste gas by the photo-Fenton reaction in a bubble column, *Chem. Eng. Sci.* 100 (2013) 212–224.
[8] D.D. McClure, Z.H. Zheng, G.Y. Hu, J.M. Kavanagh, Towards *in situ* product recovery for bubble column bioreactors, *Chem. Eng. J.* 393 (2020) 124745.
[9] V. Hecht, D. Brebbermann, P. Bremer, W.D. Deckwer, Cometabolic degradation of trichloroethylene in a bubble column bioscrubber, *Biotechnol. Bioeng.* 47 (4) (1995) 461–469.
[10] X. Wang, J.P. Wen, X.Q. Jia, CFD modelling of transient performance of toluene emissions biodegradation in bubble column, *Biochem. Eng. J.* 48 (1) (2009) 42–50.
[11] K. Muroyama, K. Imai, Y. Oka, J. Hayashi, Mass transfer properties in a bubble column associated with micro-bubble dispersions, *Chem. Eng. Sci.* 100 (2013) 464–473.
[12] F. Möller, C. Lavetty, E. Schleicher, M. Löschau, U. Hampel, M. Schubert, Hydrodynamics, mixing and mass transfer in a pilot-scale bubble column with dense internals, *Chem. Eng. Sci.* 202 (2019) 491–507.
[13] M.K.H. Al-Mashhadani, S.J. Wilkinson, W.B. Zimmerman, Airlift bioreactor for biological applications with microbubble mediated transport processes, *Chem. Eng. Sci.* 137 (2015) 243–253.
[14] R. Bannari, A. Bannari, B. Selma, P. Proulx, Mass transfer and shear in an airlift bioreactor: Using a mathematical model to improve reactor design and performance, *Chem. Eng. Sci.* 66 (10) (2011) 2057–2067.
[15] K. Wadaugsorn, S. Limtrakul, T. Vatanatham, P.A. Ramachandran, Hydrodynamic behaviors and mixing characteristics in an internal loop airlift reactor based on CFD simulation, *Chem. Eng. Res. Des.* 113 (2016) 125–139.
[16] M. Ibrahim, T. Saeed, F.R. Bani, S.N. Sedeh, Y.M. Chu, D. Toghraie, Two-phase analysis of heat transfer and entropy generation of water-based magnetite nanofluid flow in a circular microtube with twisted porous blocks under a uniform magnetic field, *Powder Technol.* 384 (2021) 522–541.
[17] M. Torabi, M. Torabi, M.E. Yazdi, G.P. Peterson, Fluid flow, heat transfer and entropy generation analyses of turbulent forced convection through isotropic porous media using RANS models, *Int. J. Heat Mass Transf.* 132 (2019) 443–461.
[18] W. Wang, Y.N. Zhang, J. Liu, B.X. Li, B. Sundén, Numerical investigation of entropy generation of turbulent flow in a novel outward corrugated tube, *Int. J. Heat Mass Transf.* 126 (2018) 836–847.
[19] H.J. Feng, L.G. Chen, Z.H. Xie, F.R. Sun, "Disc-point" heat and mass transfer constructal optimization for solid–gas reactors based on entropy generation minimization, *Energy* 83 (2015) 431–437.
[20] Q. Li, X.G. Yuan, P. Neveu, G. Flamant, L.G. Luo, A novel optimization approach to convective heat transfer enhancement for solar receiver, *Chem. Eng. Sci.* 116 (2014) 806–816.
[21] X.P. Cao, S.K. Jia, J.M. Avellaneda, Y.Q. Luo, X.G. Yuan, G. Flamant, K.T. Yu, An optimization method to find the thermodynamic limit on enhancement of solar thermal decomposition of methane, *Int. J. Hydrog. Energy* 44 (31) (2019) 16164–16175.
[22] S.K. Jia, C. Zhang, X.G. Yuan, K.T. Yu, An optimization approach to find the thermodynamic limit on convective mass transfer enhancement for a given viscous dissipation, *Chem. Eng. Sci.* 146 (2016) 26–34.
[23] V. Yakhot, S.A. Orszag, Renormalization group analysis of turbulence. I. Basic theory, *J. Sci. Comput.* 1 (1) (1986) 3–51.
[24] M. Ishii, N. Zuber, Drag coefficient and relative velocity in bubbly, droplet or particulate flows, *AIChE J.* 25 (5) (1979) 843–855.
[25] C. Zhang, X.G. Yuan, Y.Q. Luo, G.C. Yu, Prediction of species concentration distribution using a rigorous turbulent mass diffusivity model for bubble column reactor simulation part I: Application to chemisorption process of CO_2 into NaOH solution, *Chem. Eng. Sci.* 184 (2018) 161–171.
[26] K.M. Dhanasekharan, J. Sanyal, A. Jain, A. Haidari, A generalized approach to model oxygen transfer in bioreactors using population balances and computational fluid dynamics, *Chem. Eng. Sci.* 60 (1) (2005) 213–218.
[27] G.F. Andrews, Inhibitory growth of bacterial cultures, *Biotechnol. Bioeng.* 44 (1968) 707–719.
[28] A.G. Livingston, Biodegradation of 3, 4-dichloroaniline in a fluidized bed bioreactor and a steady-state biofilm Kinetic model, *Biotechnol. Bioeng.* 38 (3) (1991) 260–272.
[29] C.S. Lo, S.J. Hwang, Dynamic behavior of an internal-loop airlift bioreactor for degradation of waste gas containing toluene, *Chem. Eng. Sci.* 59 (21) (2004) 4517–4530.
[30] J.E. Bailey, D.F. Ollis, Biochemical Engineering Fundamentals, McGrawHill, New York, 1986.
[31] W. Feng, J.P. Wen, X.Q. Jia, Q. Yuan, Y. Sun, C.Y. Liu, Modeling for local dynamic behaviors of phenol biodegradation in bubble columns, *AIChE J.* 52 (8) (2006) 2864–2875.
[32] X. Wang, X.Q. Jia, J.P. Wen, Transient modeling of toluene waste gas biotreatment in a gas–liquid airlift loop reactor, *Chem. Eng. J.* 159 (1–3) (2010) 1–10.
[33] X.Q. Jia, J.P. Wen, H.L. Zhou, W. Feng, Q. Yuan, Local hydrodynamics modeling of a gas–liquid–solid three-phase bubble column, *AIChE J.* 53 (9) (2007) 2221–2231.